KLOE NOTE n^{o}194

August 2, 2004

MC generators for radiative kaon decays

C.Gatti

Univ. di Roma "La Sapienza", I.N.F.N. - sez. Roma1

Abstract

For high precision measurements of k decays, the presence of radiated photons cannot be neglected. The MC simulations must include the radiative corrections in order to compute the correct event counting and efficiency calculations. This memo shows how this can be done for the decays $K^0 \to \pi\pi$, $K^0 \to \pi e\nu$, $K^0 \to \pi\mu\nu$, $K^0 \to \pi^+\pi^-\pi^0$, $K^\pm \to \pi\pi$, $K^\pm \to e\nu$, $K^\pm \to \mu\nu$, $K^\pm \to \pi e\nu$, $K^\pm \to \pi\mu\nu$, and $K^\pm \to \pi^\pm\pi^0\pi^0$.

Contents

1 Introduction

Many KLOE measurements on k decays have reached a statistical error close to 1% or less. With such precision, the presence of radiated photons, i.e., radiative corrections, cannot be neglected anymore. Furthermore, the treatment of the radiative corrections is explicitly required for the extraction of many physical quantities, such as the CKM matrix element V_{us} and the phase shifts $\delta_0 - \delta_2$. Hence, the radiated photon must be included in Monte Carlo (MC) simulations.

There are two aspects of a measurement which are affected by the presence of a radiated photon: the geometrical acceptance and the counting of the events. For instance, in the analysis of $K_S \to \pi e \nu$ decays, the events are inside the acceptance when both the pion and the electron reach the calorimeter. The MC distribution of the photon energy is shown in the left panel of Fig. 1, while the relative acceptance as a function of the photon energy E_γ is shown in the right panel. If the presence of the photon is neglected, the acceptance is overestimated by $\sim 1\%$.

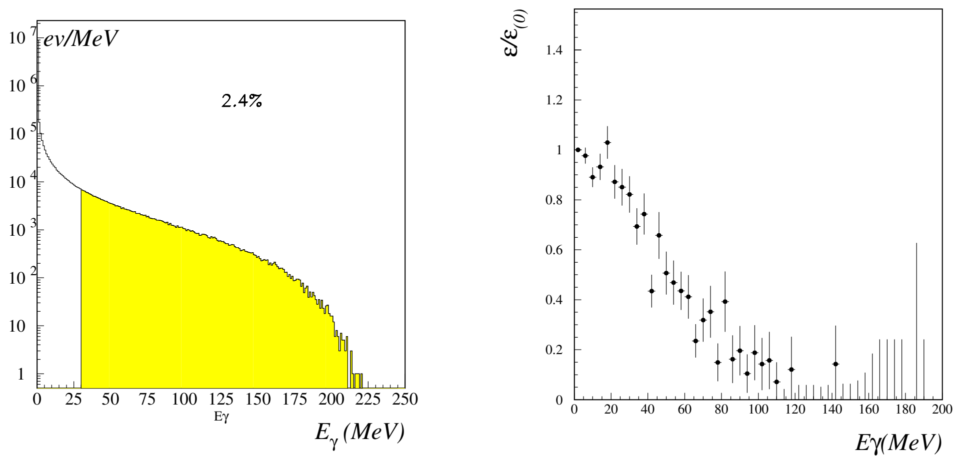

Figure 1: Left: energy spectrum for $K^0 \to \pi e \nu \gamma$ MC decays. 2.4% of the events have $E_\gamma > 30$ MeV. Right: acceptance as a function of the photon energy, normalized to the value for $E_\gamma = 0$.

In the same analysis the counting of the events is obtained from the distribution of the missing energy minus the missing momentum, $E_{miss} - p_{miss}$. The MC distributions for signal and background are used to fit the data distribution. In a previous study of $K_S \to \pi e \nu$ decays [1], the radiated photon was not included in the MC simulation, and a lack of MC events is visible in the fit, shown in the left panel of Fig. 2, in the region between 5 and 15 MeV. When photon emission is included in the MC simulation, the lack of events is recovered as shown on the right panel. The number of counted events changes in the two cases.

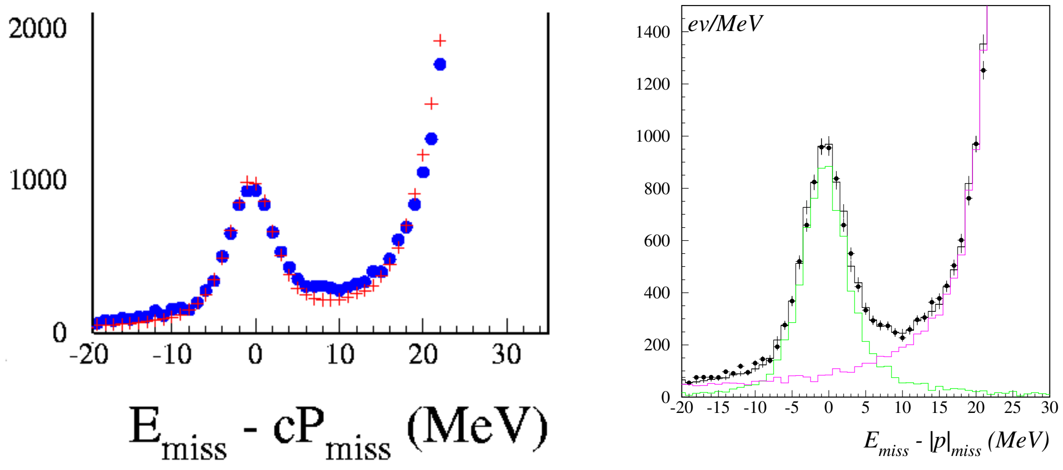

Figure 2: Fit to the $E_{miss} - p_{miss}$ distribution for a previous analysis (Left, dots are data and crosses are MC) in which the simulation of the radiated photon was not included, and for the new analysis (Right, dots are data and histograms are MC) in which the complete $K^0 \to \pi e \nu \gamma$ simulation is used.

Similar considerations applied to other analyses of the decays of neutral and charged kaons, led to the need for a complete simulation of such decays.

In this paper the method used to simulate these decays is described. For each decay some relevant distributions are shown and some comparisons are made to theoretical and experimental results, in order to establish the correctness of the various approximations and to ensure that there are no big errors (bugs) in the codes.

2 Bremsstrahlung and infrared divergences

The amplitude M^{Brem} for the process $P^0 \to a^+a^-\gamma$ with the emission of a "soft" photon ($E_\gamma/E_{CM} \ll 1$ where E_{CM} is the center of mass energy) is related to the amplitude M^0 for the process $P^0 \to a^+a^-$ by the relation [2]

$$M^{Brem} = e\left(\frac{p^+\cdot\epsilon}{p^+\cdot k} - \frac{p^-\cdot\epsilon}{p^-\cdot k}\right) M^0,$$

where p^+ and p^- are the momenta of the charged particles, and k and ϵ are the momentum and polarization of the photon. The differential decay width is related to the decay width for the process without photon emission by

$$d\Gamma_{Brem} = \Gamma_0 \frac{\alpha}{(2\pi)^2} \sum_{pol} \left|\frac{p^+\cdot\epsilon}{p^+\cdot k} - \frac{p^-\cdot\epsilon}{p^-\cdot k}\right|^2 \frac{d^3k}{k}. \tag{1}$$

The total decay width for soft photon emission is obtained by integrating the photon energy up to a cutoff value E_γ, and integrating the solid angle in the limit $\mathbf{p}^+ = -\mathbf{p}^- = \mathbf{p}$:

$$\Gamma_{Brem} = \Gamma_0 b \int_0^{E_\gamma} \frac{dk}{k} \tag{2}$$

where b is:

$$b = \left(\frac{-2\alpha}{\pi}\right)\left[1 - \frac{1+\beta^2}{2\beta}\ln\frac{1+\beta}{1-\beta}\right];$$

and β is the particle velocity in the limit of $k = 0$:

$$\beta = \frac{p}{E}.$$

This decay width is infinite. A finite value is obtained only by summing the decay widths for the radiative and non-radiative processes calculated to the same order in α [3]:

$$\Gamma_{TOT} = \Gamma_0 + \Gamma_{Brem} = \Gamma_0(1 - b\ln\frac{E_{CM}}{\lambda} + c_0) + \Gamma_0 b \ln\frac{E_\gamma}{\lambda} = \Gamma_0(1 + b\ln\frac{E_\gamma}{E_{CM}} + c_0), \tag{3}$$

where λ is a cutoff, E_{CM} is the center of mass energy, and c_0 is a finite constant of order α. This result can be generalized to the presence of any number of photons, by considering the terms in Eq. (3) as the first two terms of the series:

$$\Gamma_{TOT} = \Gamma_0(1 + b\ln\frac{E_\gamma}{E_{CM}} + \frac{1}{2!}(b\ln\frac{E_\gamma}{E_{CM}})^2 + \cdots)(1+\widetilde{c}_0) = \Gamma_0\left(\frac{E_\gamma}{E_{CM}}\right)^b(1+\widetilde{c}_0).$$

The differential decay width is obtained by differentiating with respect to E_γ:

$$\frac{d\Gamma_{TOT}}{dE_\gamma} = \Gamma_0 b(1+\widetilde{c}_0)\left(\frac{E_\gamma}{E_{CM}}\right)^{b-1} = \frac{d\Gamma_{Brem}}{dE_\gamma}\left(\frac{E_\gamma}{E_{CM}}\right)^b, \tag{4}$$

where in the last step, the term $\widetilde{c}_0$ is neglected with respect to 1. Eq. (4) describes the correct energy spectrum for the radiated soft photon, and shows that it is obtained from the decay width ($d\Gamma_{Brem}/dE_\gamma$) in Eq. (2) by multiplying by the factor $(E_\gamma/E_{CM})^b$.

A more general and rigorous derivation of Eq. (4) is given in Ref. [4]. The factor b is given by:

$$b = -\frac{1}{8\pi^2}\sum_{mn}\eta_m\eta_n e_m e_n \beta_{mn}^{-1}\ln\frac{1+\beta_{mn}}{1-\beta_{mn}}, \tag{5}$$

where m and n run over all the external particles, e_n is the charge of the particle n, $\eta = +1$ or -1 for an outgoing or incoming particle, and β_{mn} is the relative velocity of the particles n and m in the rest frame of either:

$$\beta_{mn} = \left[1 - \frac{m_n^2 m_m^2}{(p_n\cdot p_m)^2}\right]^{1/2}. \tag{6}$$

3 MC simulation for radiative decays

While for a complete MC simulation, the decay width for all values of E_γ is needed, the relation in Eq. (4) is true for only soft-photon emission. However, the value of the exponent b, which is of order α, is about 0.01. Hence, while $(E_\gamma/E_{CM})^b$ is a big correction for $E_\gamma \to 0$, its value is close to 1 when $E_\gamma \to E_{CM}$, as shown in Fig. 3. Therefore, if $d\Gamma_{Brem}/dE_\gamma$ is used for the complete decay width for the emission of a photon at order α, and not its approximation for low energies in Eq. (2), the decay width in Eq. (4) should represent a good approximation for the entire energy spectrum.

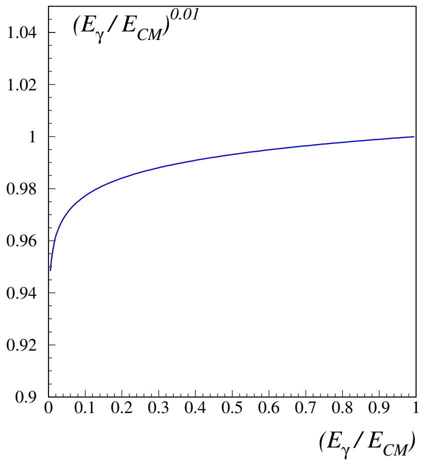

Figure 3: Correction to the decay width ($d\Gamma_{Brem}/dE_\gamma$) when $b = 0.01$.

In summary, the recipe for writing the amplitude for the process $i \to f\gamma$ is the following:

1) Calculate the b factor using Eq. (5).
2) Calculate the amplitude $M_{i\to f\gamma}$ at order α.
3) Fix the divergence in the squared amplitude by multiplying by $(E_\gamma/E_{CM})^b$:

$$|M_{i\to f\gamma}|^2_{noIR} = |M_{i\to f\gamma}|^2\,(E_\gamma/E_{CM})^b. \tag{7}$$

3.1 Sampling technique

There are mainly two ways to sample a random variable according to its distribution: the *acceptance-rejection* (Von Neumann) method and the *inverse transform* method [5]. The first method is usually applied in its simplest version, the *hit-or-miss* method. This method is however very inefficient for distributions with strong peaks. Moreover, it cannot be used if the maximum of the distribution is infinite, i.e. for divergent distributions. On the

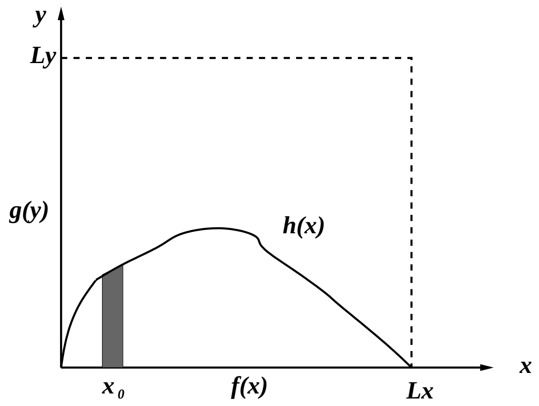

Figure 4: The generalized acceptance-rejection method.

other hand, the inverse-transform method is very efficient and can be applied to divergent distributions, but it requires the cumulative distribution to be calculated and inverted, which is not always possible.

In general, a combination of the two methods must be used, for instance using the following generalized acceptance-rejection method: the variables x and y are sampled according to the distribution functions $f(x)$ and $g(y)$, respectively, and the sampled value x_0 is accepted if $y_0 < h(x_0)$ (Fig. 4). Then the probability distribution for the variable x_0 is given by the following:

$$
\begin{aligned}
P(x_0) &= \frac{f(x_0)\int_0^{h(x_0)} g(y)\, dy}{\int_0^{L_x} f(x)\int_0^{h(x)} g(y)\, dy\, dx} \qquad (8)\\
\int_0^{L_x} f(x)dx &= 1\\
\int_0^{L_x} h(x)dx &= 1\\
\int_0^{L_y} g(y)dx &= 1.
\end{aligned}
$$

The hit-or-miss method is the particular case in which $f(x)$ and $g(y)$ are flat distributions, leading to $P(x_0) = h(x_0)$. If only $g(y)$ is a flat distribution the general acceptance-rejection method is obtained:

$$P(x_0) = \frac{f(x_0)h(x_0)}{\int_0^{L_x} f(x)h(x)\, dx}. \qquad (9)$$

This relation is very useful for samplings of random variables whose distributions can be split into a divergent and a finite part. This is the case for the radiated-photon energy. In fact, the differential decay width is of the type

$$\frac{d\Gamma}{dk} = \left(\frac{E_{CM}}{k}\right)^{1-b} F(k),$$

where $F(k)$ is a polynomial function of k. Due to the divergent factor the hit-or-miss method cannot be used. However, the generalized method can be used by splitting the decay width into a divergent part, $(E_{CM}/k)^{1-b}$, and a finite part, $F(k)$, corresponding to $f(x)$ and $h(x)$ in Eq. (9), respectively. Then, a value k_0 for the energy is obtained according to the distribution $(b/k_{max})(k_{max}/k)^{1-b}$, where k_{max} is the maximum photon energy, using the inverse-transform method:

$$k_0 = k_{max} \cdot p^{1/b} \qquad (10)$$

where p is sampled randomly between 0 and 1. Finally, the value k_0 is accepted if $y_0 < F(k_0)$, where y_0 is sampled according to a flat distribution between 0 and $F_{max}(k)$.

This method can be generalized to the presence of more kinematical variables. For instance, Eq. (1) depends on the angle between the photon and the particle which emits it, through the factor coming from the particle propagator:

$$\frac{1}{(p-q)^2-m^2} = \frac{1}{2p\cdot q} = \frac{1}{2k}\frac{1}{E-p\cos\theta}. \tag{11}$$

In this case, the decay width is of the type

$$\frac{d^2\Gamma}{dk d\cos\theta} = \left(\frac{E_{CM}}{k}\right)^{1-b} \frac{1}{E-p\cos\theta} F(k,\cos\theta).$$

One possibility is to sample the energy k as in the previous case and $\cos\theta$ according to a flat distribution, and to accept the events if $y_0 < F(k_0, \cos\theta_0)/(E - p\cos\theta_0)$. However, if the particle had a small mass m, such as an electron, the new factor would give rise to a huge peak in the decay width, corresponding to the collinear emission of the photon, and the sampling would be very inefficient. Therefore, the factor $1/(E - p\cos\theta)$ must be used to sample E and $\cos\theta$, or some combination of the two, by calculating the inverse of its cumulative. In this way, the events are accepted if $y_0 < F(k_0, \cos\theta_0)$, avoiding the problem of the collinearity peak.

In general, the divergences and peaks of the differential decay width have to be identified by inspection, and integrated by choosing the proper set of kinematical variables. This choice depends on the type of divergences present, on the correlations between these divergences, and on the number of available variables. The number of available variables depends on the number of particles in the final state: two for a three body decay, and five for a four body decay [1]. There are mainly to types of divergencies as described above: a divergence for the photon energy and one or more collinearity peaks. However, other peaks could arise in the photon spectrum due to structure-dependent (SD) terms in the amplitude. The correlations arise when a divergent or peaked factor depends on more than one variable, as in the factor $1/(E - p\cos\theta)$. In this case, if the variables E and $\cos\theta$ are available, both can be used to integrate the peaked factor [see Sec. (4.2)]. Otherwise, the combination $x = (E - p\cos\theta)$ can be used [see Sec. (4.7)]. Another correlation arises in the factor $(E_{CM}/k)^{1-b}$ for four body decays, since the factor b is not a constant, but depends on the scalar product between the two momenta of the charged particles through the factor β_{mn} [Eq. (6)]. Therefore, one of the integration variables must be related to this scalar product.

[1] Neglecting irrelevant angles.

In summary, the recipe for sampling the kinematical variables for the process $i \to f\gamma$ is the following:

1) Identify divergences and peaks in the differential decay width.

2) Choose the proper variables for integrating these factors, and write the correct phase space factor using these new variables.

3) Split the decay width in divergent-peaked factors D_i and a polynomial factor F:

$$\frac{d^n\Gamma}{dx_1 \cdots dx_n} = \prod_i D(x_1 \cdots x_n)_i F(x_1 \cdots x_n)$$

3) Sample the variables $x_{0,i}$ according to the functions D_i using the method of the inverse of the cumulative.

4) Impose the boundary of the Dalitz-plot.

5) Sample a random variable y between 0 and F_{max} and accept the event only if $y < F(x_{0,1} \cdots x_{0,n})$.

4 MC generators

In this section the MC generators for the radiative decays of the kaons are discussed. These generators are obtained using the method described in the previous sections. The choice of the integration variables is explained, and simulated distributions are compared with theoretical and experimental results.

4.1 $K^0 \to \pi^+\pi^-\gamma$

The decay width for this process is given by

$$d\Gamma_{Brem} = |A_0|^2 \frac{-\alpha}{(2\pi)^2} \left| \frac{p^+}{p^+ \cdot k} - \frac{p^-}{p^- \cdot k} \right|^2 \left(\frac{k}{M_K} \right)^b d\Phi_3, \qquad (12)$$

where $p_\pm$ are the 4-momenta of the charged pions, $d\Phi_3$ is the phase space factor, and A_0 is a constant [2]. The infrared divergence has been cured with the factor $(k/M_K)^b$. The factor b, given by Eq. (5), is equal to:

$$b = -\frac{2\alpha}{\pi}\left[1 - \frac{1}{2\beta_\pm}\ln\frac{1+\beta_\pm}{1-\beta_\pm}\right]$$

where

$$\beta_\pm = \sqrt{1 - \frac{4m_\pi^4}{(M_k^2 - 2m_\pi^2)^2}}.$$

Since the pion mass is not small compared to the kaon mass, there are no collinearity peaks, and the only divergent factor is that due to the photon energy.

The photon energy k and $\cos\theta$, the cosine of the angle between the photon and a pion, are chosen as integration variables. $\cos\theta$ is sampled from a flat distribution between -1 and $+1$, and k is sampled between 0 and $k_{max} = (M_k^2 - 4m_\pi^2)/2M_k$ according to Eq. (10). If $k > k_{max}(\cos\theta)$, the Dalitz-plot boundary (see left panel of Fig. 5), the event is rejected.

Finally the events are weighted with the polynomial part of Eq. (12):

$$h(k, \cos\theta) = \left|\frac{p^+}{p^+\cdot\hat{k}} - \frac{p^-}{p^-\cdot\hat{k}}\right|^2 \frac{d\Phi_3}{dk\,d\cos\theta}.$$

The simulated photon spectrum is shown in the right panel of Fig. 5. The fraction of events in which a photon has energy greater than 20 MeV (50 MeV) is equal to 7.00×10^{-3} (2.54×10^{-3}) in excellent agreement with the measured value $(7.10 \pm 0.22) \times 10^{-3}$ ($(2.56 \pm 0.09) \times 10^{-3}$), and that from theoretical predictions 7.01×10^{-3} (2.56×10^{-3}) for the K_s [3] (see Ref. [6]).

[2]All multiplicative constant factors are irrelevant for the sampling of the variables.

[3]These numbers refers only to the inner bremsstrahlung (IB) term. However, the K_L has a non-negligible contribution due to a direct emission (DE) term. This term, which is not infrared divergent, was already included in the simulation by T. Spadaro.

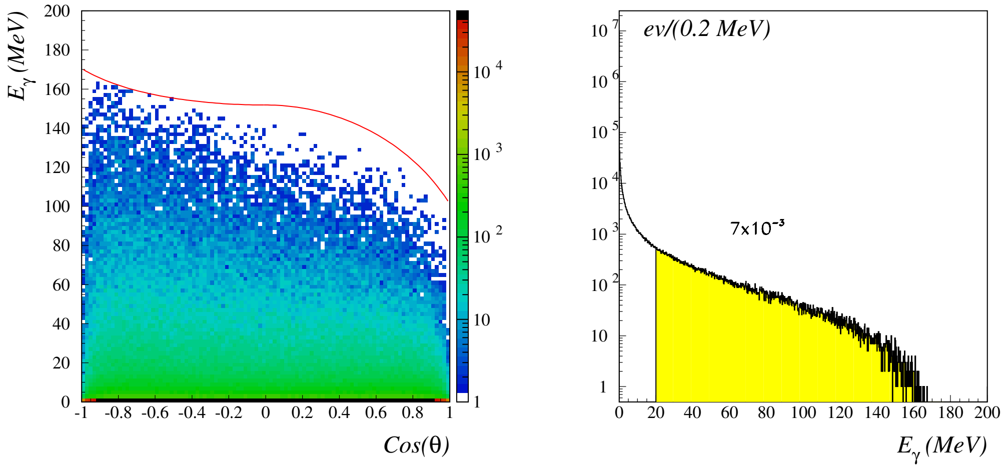

Figure 5: Left: Distribution of the simulated events in the plane $(k, \cos\theta)$. The superimposed curve shows the boundary of the physical region $k_{max}(\cos\theta)$. Right: Energy spectrum of the photon. The fraction of events with $E_\gamma > 20$ MeV is 7×10^{-3}.

4.2 $K^0 \to \pi^+ e^- \overline{\nu}\gamma$

The amplitudes for the radiative semileptonic decays of charged and neutral kaons are given in Ref. [7]. The hadronic current depends on vector and axial tensors which are calculated using chiral perturbation theory (CHPT). The tree level amplitudes to lowest order in p^2 are used for the MC simulation here. At lowest order in CHPT, the hadronic current is given by:

$$< \pi(p')|J^\mu|K(p) >= \frac{1}{\sqrt{2}}(p' + p)^\mu,$$

corresponding to the form factors $f_+ = 1$ and $f_- = 0$. Since for K_{e3} decays, the presence of the form factor f_- can be neglected, the correct amplitude is obtained by multiplying by the known expression for $f_+(t)$. For $K_{\mu3}$ decays the form factor f_- is not suppressed; however, as a first approximation, only the $f_+(t)$ factor is included in the simulation as for K_{e3}.

The differential decay width has a divergence due to the emitted photon and a collinearity peak due to the small mass of the electron. Moreover, the exponent b is not a constant but depends on the invariant mass $M_{\pi e}$ of the pion-electron system [4]. Choosing as integration variables k, $M_{\pi e}$, the electron energy E, the cosine of the angle between the photon and the electron $\cos\theta$, and the azimuthal angle of the pion with respect to the electron ϕ_π, the decay width is factorized in the following way:

$$d\Gamma = b(M_{\pi e})\left(\frac{M_K}{k}\right)^{1-b(M_{\pi e})}\frac{1}{E-p\cos\theta}F(k,\cos\theta,E,M_{\pi e},\phi_\pi)d\Phi_4, \tag{13}$$

where

$$F = |A|^2 k(E-p\cos\theta)/b. \tag{14}$$

The first factor on the right-hand side of Eq. 13 is used to sample $M_{\pi e}$ and k. It can be written as:

$$\begin{aligned} P(k,M) &= P(k|M)\times P(M) \\ P(k|M) &= \frac{b(M_K/k)^{1-b}}{\int_0^{k_{max}(M)} b(M_K/k)^{1-b}dk} \\ P(M) &= \frac{1}{N}\int_0^{k_{max}(M)} b(M_K/k)^{1-b}dk \end{aligned}$$

where $P(k|M)$ is the conditional density function of k given $M_{\pi e}$, and $P(M)$ is the marginal density of $M_{\pi e}$, which represents the probability density of $M_{\pi e}$ for unknown k. N is a normalization factor and $k_{max}(M)$ is the maximum photon energy for a given $M_{\pi e}$. Calculating the integrals:

$$P(k|M) = \frac{b}{k_{max}(M)}\left(\frac{k}{k_{max}(M)}\right)^{b-1} \tag{15}$$

$$P(M) = \frac{M_K}{N}\left(\frac{k_{max}(M)}{M_K}\right)^{b}. \tag{16}$$

Therefore, $M_{\pi e}$ is sampled according to $P(M)$ by performing an hit-or-miss. Then, k is sampled according to Eq. (10) where $k_{max} = k_{max}(M) = (M_k^2 - M_{\pi e}^2)/(2M_k)$ (see Fig. 6, left panel).

[4]It has been observed that the exponent b could be a function of $M_{\pi e}$ *before* the emission of the photon, and hence of the neutrino energy. Clearly the two definitions are identical for soft photons. Both approximations were tried and no significant differences were observed.

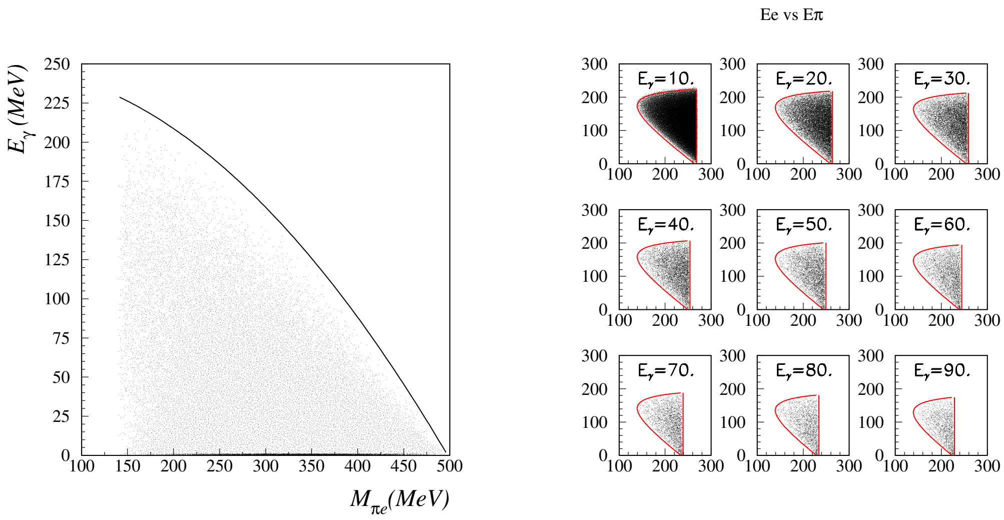

Figure 6: Left: Photon energy in $K^0 \to \pi e\nu\gamma$ decays as a function of the invariant mass of the pion and electron. Right: Dalitz-plot in the $\pi e\nu$ C.M. system for different photon energies.

A similar procedure is used to sample E and $\cos\theta$ according to $1/(E - p\cos\theta)$:

$$\begin{aligned}
P(\cos\theta, E) &= P(\cos\theta|E) \times P(E) \\
P(\cos\theta|E) &= \frac{p}{(E - p\cos\theta)\log\frac{E+p}{E-p}} \\
P(E) &= \frac{1}{p}\log\frac{E+p}{E-p}
\end{aligned}$$

where a rectangular boundary is assumed. Both distributions can be integrated and inverted, allowing efficient sampling of the variables.

In order to reject the events outside the kinematical region, the pion and electron energies in the $\pi e\nu$ CM frame are required to lie within the Dalitz-plot boundary, as shown in the right panel of Fig. 6.

Finally, the events are weighted with the polynomial part of the distribution using the hit-or-miss procedure. The energy distribution of the photon is shown in Fig. 1. The ratio

$$R^0 = \frac{\Gamma(K^0_{e3\gamma}, E_\gamma > E, \theta_{e\gamma} > \theta)}{\Gamma(K^0_{e3})}, \tag{17}$$

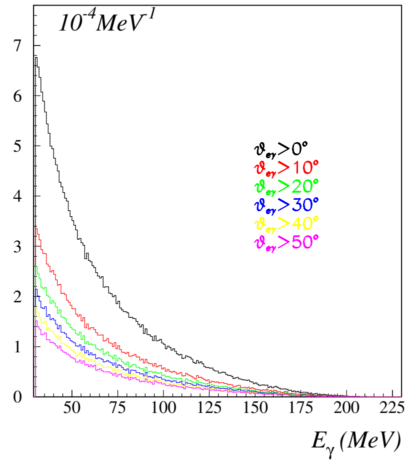

Figure 7: Photon spectrum for $K^0_{e3\gamma}$ decays. Compare with Fig. 1 in Ref. [8].

for several angles and energies is shown in Tab. 1 and in Fig. 7 for the MC simulation, and in Tab. 2 as obtained from calculations in Ref. [8]. The agreement is good. The definition of R^0 is slightly different in Tab. 1 and in Tab. 2. In the former case $\Gamma(K^0_{e3})$ refers to the total decay amplitude for physical (radiative) decays, while in the latter case it refers to the theoretical three-body decay amplitude. However, the difference between the two should affect the ratios only to order α.

Similar results are obtained in Ref. [9] as shown in Tab. 3. The differences are at the level of $1-2\%$, and are partially due to the different values used for the slope parameter λ_+ (ranging from 0.019 to 0.03), and to the model used to describe the direct emission (DE) component. Both have an effect at the level of 1%. The value 0.93×10^{-2} for $E > 30$ MeV and $\theta > 20^o$ in the simulation is in agreement with the tree level prediction in Ref. [7]. Furthermore, the full $O(p^4)$ prediction in Ref. [7] gives 0.98×10^{-2}. Hence, this difference should be considered as a theoretical error of the simulation. The same can be said by comparing this value with the measurement from the KTeV collaboration [10]

$$\frac{\Gamma(K^0_{e3\gamma}, E_\gamma > 30 \text{ MeV}, \theta_{e\gamma} > \theta)}{\Gamma(K^0_{e3})} = (0.908 \pm 0.014) \times 10^{-2}$$

θ/E(MeV)	10	20	30	40
0^o	4.90×10^{-2}	3.25×10^{-2}	2.36×10^{-2}	1.78×10^{-2}
10^o	2.44	1.65	1.22	0.93
20^o	1.85	1.26	0.93	0.71
30^o	1.51	1.02	0.76	0.58
40^o	1.26	0.86	0.63	0.49
50^o	1.06	0.72	0.54	0.41

Table 1: Ratios R^0 for K_{e3} decays obtained in the MC simulation.

θ/E(MeV)	10	20	30	40
0^o	4.99×10^{-2}	3.28×10^{-2}	2.37×10^{-2}	1.79×10^{-2}
10^o	2.51	1.69	1.25	0.96
20^o	1.92	1.30	0.96	0.74
30^o	1.57	1.06	0.79	0.61
40^o	1.31	0.89	0.67	0.51
50^o	1.11	0.76	0.57	0.44

Table 2: Ratios R^0 for K_{e3} decays listed in Ref. [8].

θ/E(MeV)	20	30	40
0^o	3.30×10^{-2}	2.39×10^{-2}	1.80×10^{-2}

Table 3: Ratios R^0 for K_{e3} decays obtained from Ref. [9].

θ/E(MeV)	20	30	40
0^o	0.348×10^{-2}	0.229×10^{-2}	0.155×10^{-2}

Table 4: Ratios R^0 for $K^0_{\mu 3}$ decays as obtained in the simulation.

θ/E(MeV)	20	30	40
0^o	0.339×10^{-2}	0.219×10^{-2}	0.147×10^{-2}

Table 5: Ratios R^0 for $K^0_{\mu 3}$ decays listed in Ref. [9] with $\lambda_+ = 0.03$.

which was obtained with approximately 16,000 radiative decays, and whose photon energy spectrum is consistent with inner bremsstrahlung as the only source of photons in $K_{e3\gamma}$ decays.

4.3 $K^0 \to \pi^+\mu^-\overline{\nu}\gamma$

The amplitude for this decay is the same as for the $K^0_{e3\gamma}$ decay. Since there is no collinearity peak due the lager lepton mass, the sampling technique is simplified by splitting the four-body decay into three two-body decays:

$$d\Phi_4 = d\Phi_2^{k,(\pi\mu\nu)} \cdot d\Phi_2^{\nu,(\pi\mu)} \cdot d\Phi_2^{\pi,\mu} \cdot (2\pi)^3 dM^2_{\pi\mu} \cdot (2\pi)^3 dM^2_{\pi\mu\nu}$$

where $M_{\pi\mu}$ and $M_{\pi\mu\nu}$ are the invariant masses of the $\pi\mu$ and $\pi\mu\nu$ particles, respectively. The integration variables are chosen to be the photon energy k, the $\pi\mu$ invariant mass $M_{\pi\mu}$, and the solid angles in the kaon rest frame, in the $\pi\mu\nu$ rest frame, and in the $\pi\mu$ rest frame. The photon energy and $M_{\pi\mu}$ are sampled as in the previous case, while the angles are sampled from flat distributions. All the events are now generated automatically inside the physical region. The energy distribution is shown in Fig. 8, while in Tab. 4 the fractions R^0 are shown for several photon energies. These should be compared with the values obtained in Ref. [9] and shown in Tab. 5 (using $\lambda_+ = 0.03$). The absolute differences are about 0.01%.

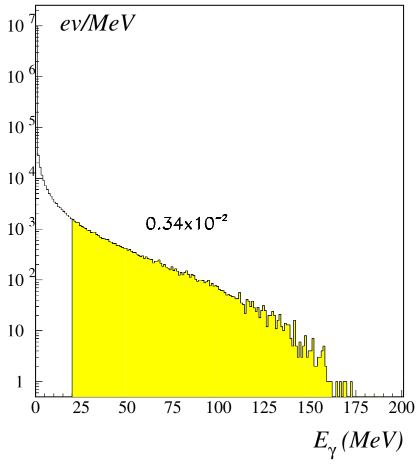

Figure 8: Photon spectrum for $K^0_{\mu 3\gamma}$ decays.

4.4 $K^0 \rightarrow \pi^+\pi^-\pi^0\gamma$

The leading term of the decay amplitude for this process is obtained from the Low theorem as follows:

$$d\Gamma_{Brem} = |A_{(3\pi)}|^2 \frac{-\alpha}{(2\pi)^2} \left| \frac{p^+}{p^+ \cdot k} - \frac{p^-}{p^- \cdot k} \right|^2 \left(\frac{k}{M_K} \right)^b d\Phi_4, \tag{18}$$

where $|A_{(3\pi)}|$ is the amplitude for the three-body decay. For the simulation of K_S and K_L decays, the usual decompositions in isospin amplitudes are used. The events are generated by the same procedure used for $K_{\mu 3}$ decays. The photon spectra are shown in Fig. 9.

4.5 $K^\pm \rightarrow \pi^\pm\pi^0\gamma$

The emission of radiation in this decay is dominated by the IB contribution, and the DE contribution can be neglected in the simulation [11]. Therefore, according to Eq. (2.3) in Ref. [4], or Eq. (1.7) in Ref. [2], the decay width for this process is given by:

$$d\Gamma_{Brem} = |A_0|^2 \frac{-\alpha}{(2\pi)^2} \left| \frac{p^+}{p^+ \cdot k} - \frac{p_K}{p_K \cdot k} \right|^2 \left(\frac{k}{M_K} \right)^b d\Phi_3, \tag{19}$$

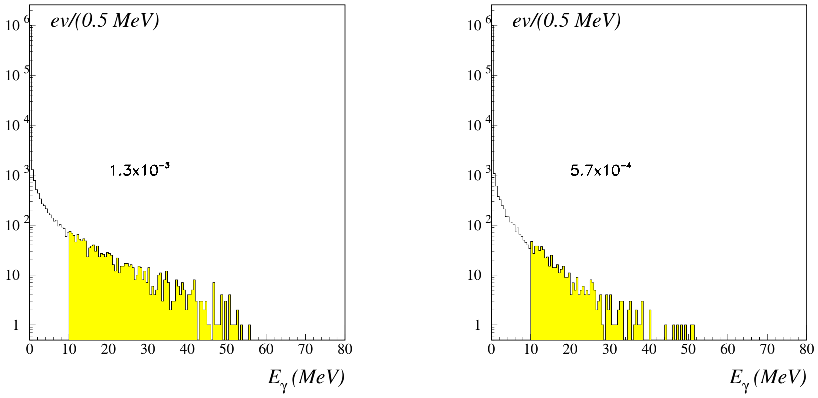

Figure 9: Photon spectrum for K_L (Left) and K_S (Right) decays into $\pi^+\pi^-\pi^0\gamma$.

where p^+ and p_K are the momenta of the charged pion and of the kaon, respectively. The sampling method and the choice of the integration variables are as described in Sec. 4.1. The exponent b has the usual expression, but with

$$\beta = \sqrt{1 - \frac{4M_K^2 m_+^2}{(M_K^2 + m_+^2 - m_0^2)^2}}.$$

The photon energy spectrum is shown in Fig. 10.

Experimental values in the region 55 MeV $< T_+ <$ 90 MeV, where T_+ is the kinetic energy of the charged pion, confirm the prediction of the IB branching ratio of 2.61×10^{-4}, and find a 1.8% contribution due to DE. The fraction of events in this region in the simulation is 1239×10^{-6}, which should be compared to the prediction:

$$R = \frac{BR(K^\pm \to \pi^\pm\pi^0\gamma, 55\text{ MeV} < T_+ < 90\text{ MeV})}{BR(K^\pm \to \pi^\pm\pi^0)} = \frac{2.61 \times 10^{-4}}{0.2113} = 1235 \times 10^{-6}.$$

4.6 $K^\pm \to \mu\nu\gamma$

The amplitude for $K \to l\nu\gamma$ decays is given in Ref. [7]. The IR divergence is cured by multiplying by $(E_\gamma/E_{CM})^b$ as usual. In this case b is a constant that depends on the charged lepton velocity in the limit of zero photon energy.

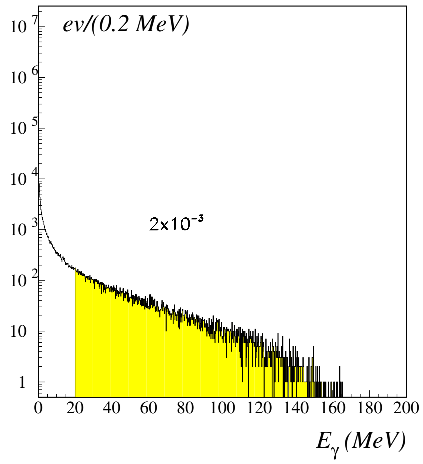

Figure 10: Photon spectrum for $K^\pm \to \pi^\pm\pi^0\gamma$ decays.

For $K^\pm \to \mu\nu\gamma$ decays, the sampling is performed as for $k \to \pi\pi\gamma$ decays, since there is no collinearity peak. The photon spectrum is shown in Fig. 11.

The radiation is dominated by the IB component. The branching ratio in the region 214.5 MeV/c $< p_\mu < 231.5$ MeV/c has been measured to be $(3.02 \pm 0.10) \times 10^{-3}$ while the prediction is 3.08×10^{-3} [7]. In the simulation, the fraction of events in this region is 4.81×10^{-3}, corresponding to a branching ratio:

$$
\begin{aligned}
& BR(K^\pm \to \mu\nu\gamma, 214.5 < p_\mu(\text{MeV/c}) < 231.5) = \\
& \qquad 4.81 \times 10^{-3} \times BR(K^\pm \to \mu\nu) \; = \; 3.05 \times 10^{-3}.
\end{aligned}
$$

4.7 $K^\pm \to e\nu\gamma$

For this decay, the collinearity peak has to be taken into account when choosing the integration variables. For a three-body decay, only two variables are available. The photon energy is chosen for integration of the IR divergence, and the variable $x = (E_e - p_e \cos\theta)/M_K$ is used for the collinearity peak factor, $1/x$. This last factor is easily integrated and inverted since the lower value of x, $x_{min} = (m_e/M_K)^2$, is greater than

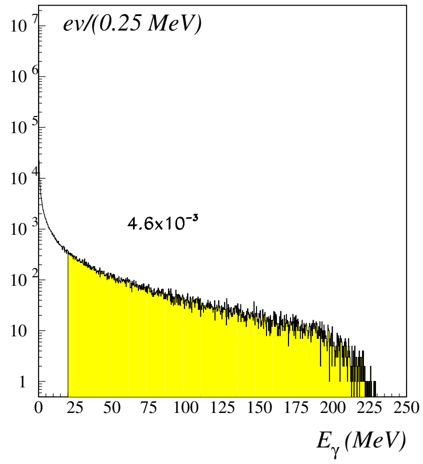

Figure 11: Photon spectrum for $K^\pm \to \mu\nu\gamma$ decays.

zero.

The photon spectrum is shown in Fig. 12. As can be seen there is a large contribution from SD terms at higher photon energies [5]. In fact, the measured branching ratio for the SD part is [12] $(1.62 \pm 0.47) \times 10^{-5}$, which is comparable to that of the K_{e2} decays $(1.55 \pm 0.07) \times 10^{-5}$. This is due to the fact that two-body K_{e2} decays, and also the IB component of the $K_{e2\gamma}$ decays, are suppressed by angular momentum conservation, which forces the electron to have the *wrong* helicity. On the other hand, the SD term corresponds to the back-to-back emission of electron and neutrino with the *correct* helicity, and the photon parallel or anti-parallel to the electron as shown in the left panel of Fig. 13. The amplitude for the SD process with the photon anti-parallel to the electron is at least one order of magnitude larger than the other SD term. This can be seen in the right panel of Fig. 13, where the SD contribution is visible at large angle between the photon and electron, while the IB contribution is visible at small angles.

[5] This contribution slows down the hit-or-miss procedure in the simulation, since it is optimized for sampling the IB component. On an AMD Athlon XP 1600+ (1.5 GHz) it takes $\sim$ 1.7 ms to generate one event, a factor 5-10 higher than the other generators.

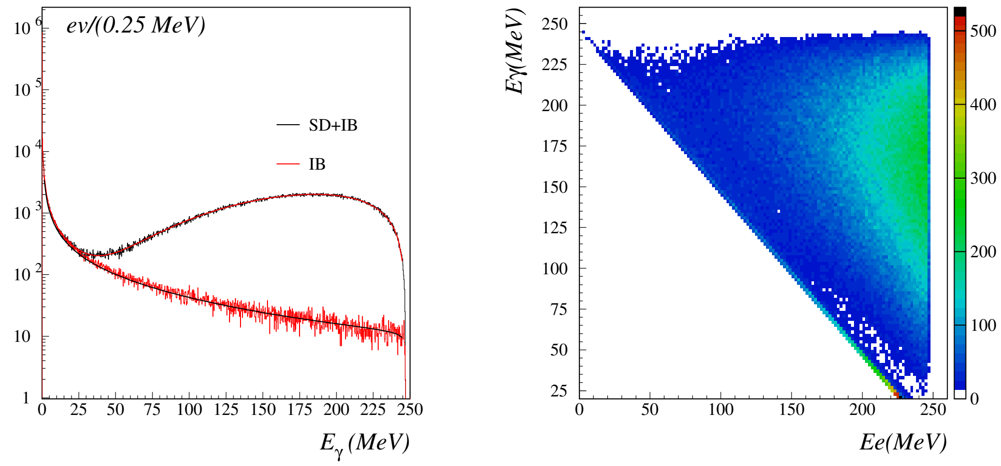

Figure 12: Left: Photon spectrum for $K^{\pm} \to e\nu\gamma$ decays. The IB (red histogram) and (IB+SD) (black histogram) spectra are shown. The theoretical spectra used to generate the events superimposed, normalized to the number of events. Right: Photon energy vs. electron energy. The line in the central region, where E_γ is anti-correlated to E_e, is due to the IB component.

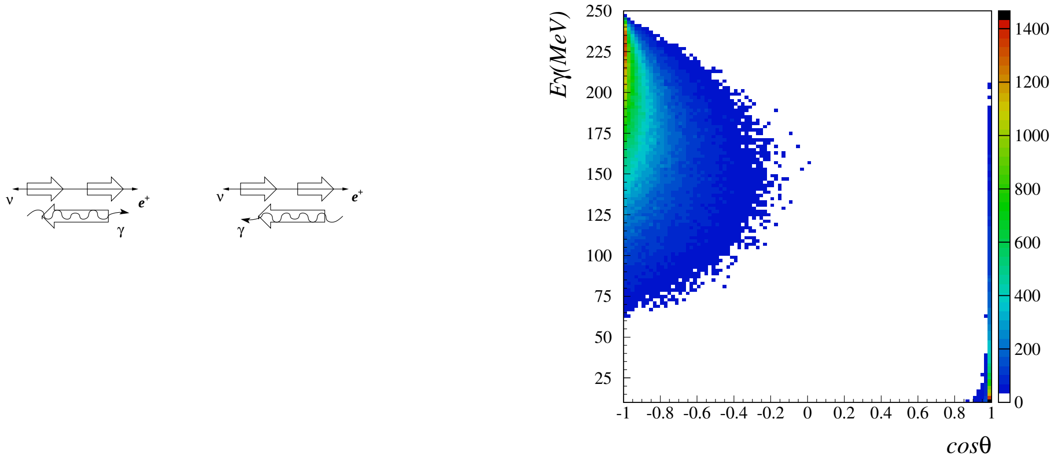

Figure 13: Left: Processes corresponding to the SD term, where the photon is parallel or anti-parallel to the electron. The latter is the dominant SD contribution. Right: Photon energy as a function of the angle between the photon and the electron. At small angles the IB term is dominant, while at large angle the SD term is dominant.

The comparison with theoretical predictions must be done with some care. In fact, in this decay there is a big contribution from IB radiative corrections, due to the presence of the monochromatic electron with an energy of 247 MeV. For instance, the expected branching ratio for the two-body decay is:

$$BR(K \to e\nu)_{2body} = (1.63 \pm 0.05) \times 10^{-5},$$

while using the ratio $\Gamma(Ke2)/\Gamma(K\mu2)$ computed in [13], which includes all the radiative corrections and the known value of $\Gamma(K\mu2)$, the expected branching ratio is:

$$BR(K \to e\nu\gamma)_{IB} = (1.57 \pm 0.05) \times 10^{-5},$$

corresponding to a 3.5% relative correction [6]. The same value (1.57×10^{-5}) is obtained by integrating the IB part of the amplitude corrected for the IR divergence as described in

[6]This difference is significant since the two errors, dominated by the knowledge of F_K and V_{us}, are completely correlated.

E_{min} - E_{max} (MeV)	$\Delta BR/BR$ (%)
1 - 10	12.9
10 - 20	9.2
20 - 30	7.9
30 - 40	7.0
40 - 50	6.3
50 - 100	5.2
100 - 246.8	3.2

Table 6: Percent difference between the $O(\alpha)$ and $O(\alpha^n)$ decay width in the energy intervals E_{min} - E_{max}.

the previous sections. The measured value [12], which includes only the IB component,

$$BR(K \to e\nu)_{2body} = (1.55 \pm 0.07) \times 10^{-5},$$

is not sensitive to this difference, even if the central value is lower than the two-body prediction.

A more significant difference is expected between the differential decay width at first order in α $d\Gamma_{IR}/dE_\gamma$, with the emission of only one photon, and that obtained by summing over all orders in α:

$$\frac{d\Gamma_{NOIR}}{dE_\gamma} = \frac{d\Gamma_{IR}}{dE_\gamma} \times (\frac{E_\gamma}{M_K})^b.$$

This is shown in Tab. 6, where the quantity

$$\frac{\Delta BR}{BR} = \frac{\Gamma_{IR}(E_{min} < E_\gamma < E_{max}) - \Gamma_{NOIR}(E_{min} < E_\gamma < E_{max})}{\Gamma_{IR}(E_{min} < E_\gamma < E_{max})}$$

is listed for different values of the energy interval. Therefore, the emission of more than one photon is not negligible, giving a relative contribution of up to 7-9% in the energy range between 10 and 40 MeV.

The contribution of the first and second order in α can be calculated using the relation

$$\Gamma(E < E_{cut}) = \Gamma_{2-body} \times (1 + b \cdot \ln\frac{E_{cut}}{M_K} + \frac{1}{2}(b \cdot \ln\frac{E_{cut}}{M_K})^2 + \cdots).$$

E_{min} - E_{max}	$\Delta(O(\alpha))$	$\Delta(O(\alpha^2))$
1 - 10	0.063	-0.0087
10 - 20	0.019	-0.0018
20 - 30	0.011	-0.00091
30 - 40	0.0078	-0.00057
40 - 50	0.0061	-0.00040
50 - 60	0.0050	-0.00030
60 - 70	0.0042	-0.00023
70 - 80	0.0036	-0.00019
80 - 90	0.0032	-0.00015
90 - 100	0.0029	-0.00013
100 - 110	0.0026	-0.00011
100 - 246.8	0.025	-0.00077
TOT	0.153	-0.0142

Table 7: Contribution to the decay width of the first and second order in α for different energy ranges. Above 1 MeV higher order terms are negligible.

In the energy interval between E_{min} and E_{max}, these are given by

$$\Delta(O(\alpha)) = b \cdot \ln \frac{E_{max}}{E_{min}}$$

and

$$\Delta(O(\alpha^2)) = \frac{1}{2} b^2 \cdot \left((\ln \frac{E_{max}}{M_K})^2 - (\ln \frac{E_{min}}{M_K})^2 \right),$$

and are shown in Tab. 7. The second-order term reduces the decay width in the energy interval between 10 and 40 MeV by a factor of about 10%.

In [7], the branching ratio for the IB component is computed for the range of electron momentum $214.5 < p_e(\text{MeV/c}) < 231.5$ (approximately $15 < E_\gamma(\text{MeV}) < 30$), and the total branching ratio for the SD part is also given [7]. These are shown in Tab. 8. These numbers must be compared with those obtained by multiplying the fraction of IB and SD

[7]The interference is negligible.

IB $O(\alpha)$ $214.5 < p_e$(MeV/c) < 231.5	SD
3.00×10^{-7}	1.51×10^{-5}

Table 8: Branching ratios obtained from the formulas in Ref. [7], p. 321.

IB $O(\alpha^n)$ $214.5 < p_e$(MeV/c) < 231.5	SD
2.75×10^{-7}	1.46×10^{-5}

Table 9: Branching ratios obtained by multiplying the fraction of events found from the MC spectra by the total branching ratio.

events found in the MC simulation by the total branching ratio obtained by integrating the theoretical decay width:

$$BR(K^+ \to e\nu\gamma) = 3.035 \times 10^{-5}.$$

The relative difference for the IB component is $\sim 9\%$, which is compatible with the expected contribution from higher orders in α as shown in Tab. 6 and Tab. 7.

The relative difference for the SD component is $\sim 3\%$. This difference is not related to higher-order terms, but to the approximation made by multiplying the entire expression for the differential decay width, and not only the IB term, by the factor $(E/M)^b$. Hence, since the SD spectrum is in the energy region between 50 and 100 MeV, a correction of this order can be expected by looking at Tab. 6. Clearly, the best way for simulating the process would be to split the IB and SD parts in two different MC generators. However, since this difference is small, and the SD contribution is known with poor accuracy ($\sim 13\%$), this is still a good approximation.

4.8 $K^\pm \to \pi e\nu\gamma$

The differential decay width for this process is of the type of Eq. 13. However, since the charged particles are now the electron and the kaon, the exponent b depends on the electron energy in the kaon rest frame. Hence, the divergent and the peaked factors include correlations between the three variables k, E, and $\cos\theta$, which must be sampled in a conditional way. Following the procedure described in Sec. 4.2, the three variables are sampled according to the following distribution

$$
\begin{aligned}
P(k, \cos\theta, E) &= P(k|\cos\theta, E) \times P(\cos\theta|E) \times P(E) \\
P(k|\cos\theta, E) &= \frac{b(E)}{k_{max}} \left(\frac{k_{max}}{k}\right)^{1-b} \\
P(\cos\theta|E) &= \frac{p}{(E - p\cos\theta)\ln{(E+p)/(E-p)}} \\
P(E) &= \frac{M_K}{N} \left(\frac{k}{M_K}\right)^{b(E)} \frac{1}{p} \ln\frac{E+p}{E-p}.
\end{aligned}
$$

The energy E is sampled with the hit-or-miss method, since the factor $(k/M_K)^{b(E)}$ cannot be integrated, while the other two variables are sampled using the inverse-transform method. The pion and neutrino energies are obtained by sampling the two angles in the $\pi\nu$ rest frame, whose CM energy depends on the three variables k, E, and $\cos\theta$, and then by boosting into the kaon rest frame. The boundaries of the kinematical region are then simply imposed by setting the correct limits on the $\pi\nu$ invariant mass. The photon spectrum is shown in Fig. 14 (left panel) together with the π-e Dalitz-plot in the $\pi e\nu$ rest frame for different photon energies. The expected boundary is superimposed, showing that all events are generated inside the physical kinematical region.

The energy spectrum for different cuts in the angle θ between the photon and the electron is shown in Fig. 15 and can be compared with Fig. 2 in Ref. [8].

The ratio $R^{\pm}$, defined in the same way as the ratio R^0 (Eq. 17), is shown in Tab. 10 for several values of the energy and the angle θ. It must be compared with theoretical predictions listed in Tab. 11 and Tab. 12. The relative differences are within 1-2%.

Similar results are obtained in Ref. [9] as shown in Tab. 12.

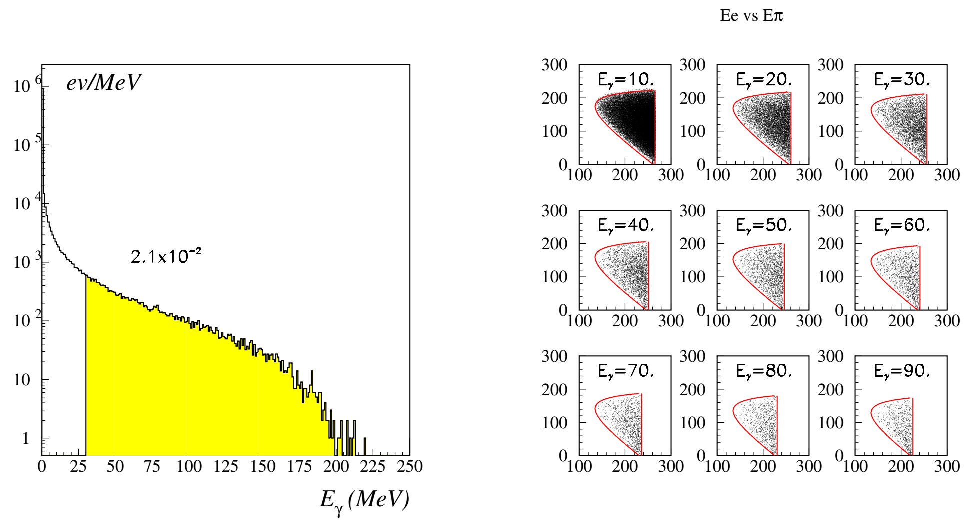

Figure 14: Left: Photon energy spectrum. Right: Dalitz-plot in the $\pi e \nu$ C.M. system for different photon energies.

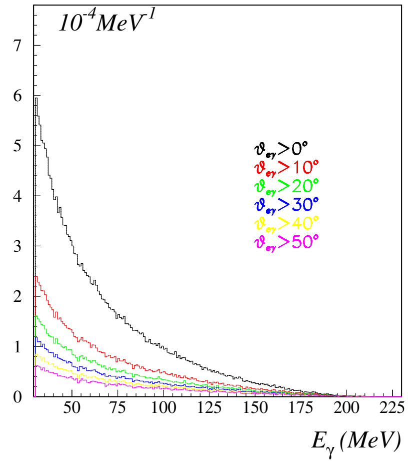

Figure 15: Photon spectrum for $K^{\pm}_{e3\gamma}$ decays. Compare with Fig. 2 in Ref. [8].

θ/E(MeV)	10	20	30	40
0^o	4.223×10^{-2}	2.825×10^{-2}	2.069×10^{-2}	1.572×10^{-2}
10^o	1.781	1.238	0.936	0.732
20^o	1.211	0.854	0.652	0.515
30^o	0.881	0.63	0.488	0.388
40^o	0.659	0.477	0.373	0.3
50^o	0.493	0.363	0.289	0.234

Table 10: Ratios $R^{\pm}$ for $K^{\pm}e3$ decays as obtained in the MC simulation.

θ/E(MeV)	10	20	30	40
0^o	4.24×10^{-2}	2.80×10^{-2}	2.03×10^{-2}	1.53×10^{-2}
10^o	1.78	1.22	0.91	0.71
20^o	1.20	0.83	0.63	0.50
30^o	0.87	0.61	0.47	0.37
40^o	0.65	0.46	0.36	0.29
50^o	0.48	0.35	0.27	0.22

Table 11: Ratios $R^{\pm}$ for $K^{\pm}e3$ decays listed in Ref. [8].

θ/E(MeV)	20	30	40
0^o	2.82×10^{-2}	2.04×10^{-2}	1.54×10^{-2}

Table 12: Ratios $R^{\pm}$ for $K^{\pm}e3$ decays obtained from Ref. [9].

θ/E(MeV)	20	30	40
0^o	1.07×10^{-3}	0.68×10^{-3}	0.46×10^{-3}

Table 13: Ratios $R^{\pm}$ for $K^{\pm}_{\mu 3\gamma}$ decays as obtained in the simulation.

4.9 $K^{\pm} \to \pi\mu\nu\gamma$

The MC generator for this decay is exactly the same as that for $K^{\pm}e3$ decays previously described. The spectrum of the photon energy is shown in Fig. 16, while the ratio $R^{\pm}$ is shown in Tab. 13, which should be compared with the values in Tab. 14. The absolute differences are about $\sim 5 \times 10^{-5}$.

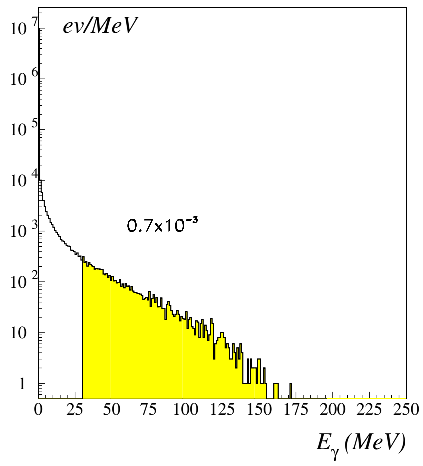

Figure 16: Photon spectrum for $K^{\pm}_{\mu 3\gamma}$ decays.

4.10 $K^{\pm} \to \pi^{\pm}\pi^0\pi^0\gamma$

The amplitude for this process is obtained from Low theorem as for the $K_0 \to 3\pi\gamma$ decays, and the generation of the events follows the same method used for $K^{\pm}\mu 3$ decays. The photon spectrum is shown in Fig. 17.

θ/E(MeV)	20	30	40
0^o	1.13×10^{-3}	0.74×10^{-3}	0.51×10^{-3}

Table 14: Ratios $R^{\pm}$ for $K^{\pm}_{\mu 3\gamma}$ decays obtained from Ref. [9].

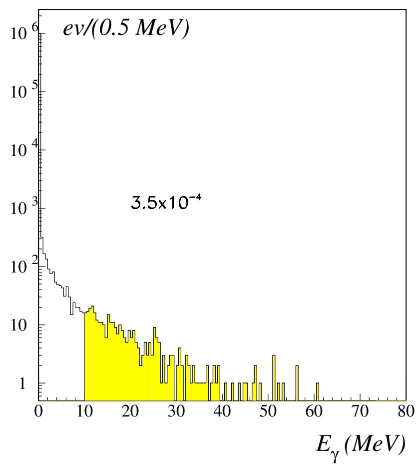

Figure 17: Photon spectrum for $K^{\pm} \to \pi^{\pm}\pi^0\pi^0\gamma$ decays.

5 Conclusions

For solving the problem of the IR divergence, the extension of the soft-photon approximation to the whole energy range, gives a satisfactory approximation for the kaon radiative decays. Only K_{e2} decays are sensitive to higher-order corrections at energies up to 50 MeV.

In $K_{\mu 3}$ decays only the form factor f_+ has been included. Furthermore, the relative difference with respect to theoretical expectations, where only f_+ is considered, is at the 5% level, as shown in the tables in Sec. 4.3 and Sec. 4.9. However the absolute differences, being less than 10^{-4}, are negligible.

6 Acknowledgments

I would like to thank Gino Isidori for many useful hints and discussions, Mario Antonelli for suggesting the method for writing the MC generators.

References

[1] C. Gatti PHD Thesis http://WWW.infn.it/thesis/PS/253-Gatti-dottorato.ps

[2] F.E. Low, Phys. Rev. **110** (1958) 974.

[3] F. Mandl, G. Shaw *Quantum Field Theory*, John Wiley & Sons.

[4] S. Weinberg, Phys. Rev. **140** (1965) 516.

[5] K. Hagiwara et al., *Monte Carlo Techniques*, Phys. Rev. **D66** (2002) .

[6] E.J. Ramberg et al., Phys. Rev. Lett. **70** (1993) 2525.

[7] J. Bijnens et al., *The second DaΦne physics handbook*, **Volume I:315**, 1995

[8] M.G. Doncel, Phys. Lett. **32B** (1970) 623.

[9] H.W. Fearing et al., Phys. Rev. Lett. **24** (1970) 189.

[10] A. Alavi-Harati et al., arXiv:hep-ex/0106062 v1

[11] S. Adler et al., Phys. Rev. Lett. **85** (2000) 4856.

[12] J. Heintze et al., Nucl. Phys. **B149** (1979) 365.

[13] M. Finkemeier, *The second DaΦne physics handbook*, **Volume I:389**, 1995